J Mol Model (2014) 20:2437
DOI 10.1007/s00894-014-2437-8

ORIGINAL PAPER

Injection, transport, absorption and phosphorescence properties of a series of platinum (II) complexes with N-heterocyclic carbenes: a DFT and time-dependent DFT study

Leijiao Li · Xiaojuan Liu · Jing Feng · Shuyan Song · Hongjie Zhang

Received: 16 June 2014 / Accepted: 25 August 2014 / Published online: 17 September 2014

Abstract The ground and excited states, charge injection/transport, and phosphorescence properties of five N heterocyclic carbine-functionalized Pt^{II} complexes were investigated by using the DFT method. By analyzing the nonradiative (k_{nr}) rate constant and energies at S_0^{opt} and T_1^{opt} states, it is possible to forecast that BC5 with the pyrrole ligand has a higher phosphorescence quantum yield than any of the other four complexes. Thus, we consider that BC5 will be an efficient phosphorescent material that has balanced electron/hole-transport performance as well as high phosphorescence quantum yield. The calculated results indicate that, for the studied complexes, the nature of the ligand strongly affected the energy of the emissive state and was able to tune the emission color. We hope that our study will aid better understanding of the structure–property relationship of phosphorescent Pt (II) complexes and provide constructive information for designing novel and highly efficient OLED materials in the future.

Keywords Density functional calculations · Electron/hole transport · Platinum · OLED

Electronic supplementary material The online version of this article (doi:10.1007/s00894-014-2437-8) contains supplementary material, which is available to authorized users.

L. Li · X. Liu · J. Feng · S. Song · H. Zhang (✉)
State Key Laboratory of Rare Earth Resource Utilization, Changchun Institute of Applied Chemistry, Chinese Academy of Sciences, 130022 Changchun, People's Republic of China
e-mail: hongjie@ciac.jl.cn

L. Li
Jilin University of Chemical Technology, 132022 Jilin, People's Republic of China

Introduction

Phosphorescent transition-metal compounds are currently of great interest as biological imaging agents, chemical sensors, and emitters for organic light-emitting diodes (OLEDs) [1–5]. Within the past decade, considerable efforts have been devoted to search for highly efficient three primary color (red, green, and blue) emitters, which are essential components for full-color displays. However, tuning of phosphorescence over the entire visible spectrum still remains a challenge. Compared to red and green emitters, which have been used successfully in OLEDs with high efficiency and stability, designing stable and efficient blue-emitting materials has encountered more obstacles owing to the wide energy gap required between the excited triplet state and the ground state. Thus, improvements to the efficiency and lifetime of blue phosphorescence materials are still vital to the success of OLEDs. Transition-metal phosphors containing N-heterocyclic carbene (NHC) ligands [6], however, show promise as a solution to the problem above. The strong ligand field of the carbene can raise the energy of nonradiative $d-d$ excited states on the metal center, increasing the energy spacing with emissive excited states and improving quantum yields [7]. Furthermore, the stability of metal–carbene bonds may also increase the operational lifetime of these materials in organic electronic devices [8–16]. Phosphorescent d^8 transition-metal complexes have been attracting increased interest for the design and synthesis of new functional molecular materials. Pt (II) complexes are typical phosphorescent materials with d^8 electronic configuration.

Many investigations of Pt (II) complexes have been reported in the past few years [17–20]. Among these reports, Wang et al. [21] reported that the introduction of boron-functionalized C^C-chelate carbine leads to

good quantum efficiency in both in CH_2Cl_2 solution and thin films. In addition, electrophosphorescent devices were fabricated by doping these complexes as emitters. They concluded that the introduction of NHC ligands improves the device, with maximum brightness of 4,165 cd cm^{-2} at 4.0 V and 2,098 cd cm^{-2} at 3.6 V for BC1 and BC2, respectively. Wang et al. [21] also performed a theoretical study on the lowest triplet state, which involves mainly HOMO to LUMO character, to gain insight into the reason for the different quantum yields observed on these complexes experimentally. Encouraged by the work by Wang et al. [21], we designed three other complexes BC3, BC4 and BC5, on the basis of the experimental structures BC1 and BC2, aimed at exploring the effects of different ligands on the electronic structures and photophysical properties of these Pt (II) complexes (shown in Fig. 1). With the development of theoretical chemistry, the reliability and accuracy of computational chemistry is becoming widely recognized. Computational chemistry has become an important auxiliary tool for experimental chemists. Therefore, one would like to predict beforehand the potential properties of possible emitters in order to screen out configurations without the desired qualities and to identify those systems worthy of testing experimentally. Indeed, computational studies can help us by providing a variety of information about some important aspects of the system under investigation.

Computational methods

The ground-state and the lowest-lying triplet excited-state geometries for each complex were optimized by using the density functional theory (DFT) and time-dependent density functional theory (TD-DFT) with the M06-2× [22], respectively. There were no symmetry constraints on these complexes. Results of the calculated vibrational frequencies for them indicate that there was no imaginary frequency on the optimized geometries, which means the geometries are the minimum points on their potential energy surface. To obtain the absorption and emission spectral properties, time dependent DFT (TD-DFT) calculations [22–25] associated with the polarized continuum model (PCM) [26–28] in dichloromethane (CH_2Cl_2) media, were performed on the basis of the optimized ground- and lowest triplet excited-state equilibrium geometries. A "double-ξ" quality basis set consisting of Hay and Wadt's effective core potentials (LANL2DZ) [29, 30] was employed for the Pt atom and a 6-31+G (d, p) basis set [31] for C, H, N, B and O atoms. All calculations were performed with the Gaussian 09 program package [32].

Results and discussion

Molecular geometries in the ground state S_0 and triplet excited state T_1

The optimized ground state geometrical structures of BC1 to BC5 in gas phase at M06-2×/LANL2DZ level are shown in Fig. 2. Selected bond lengths and angles are summarized in Table 1 and the corresponding crystal data of BC1 and BC2 obtained from experiment are also given.

The calculated results revealed that the ground state geometries of these five complexes display a slightly distorted planar construction in the [Pt (C^C) (O^O)] moiety. The carbon atom (C10 or C1) and the oxygen atom (O1 or O2) occupy the axial positions and coordinate with the center

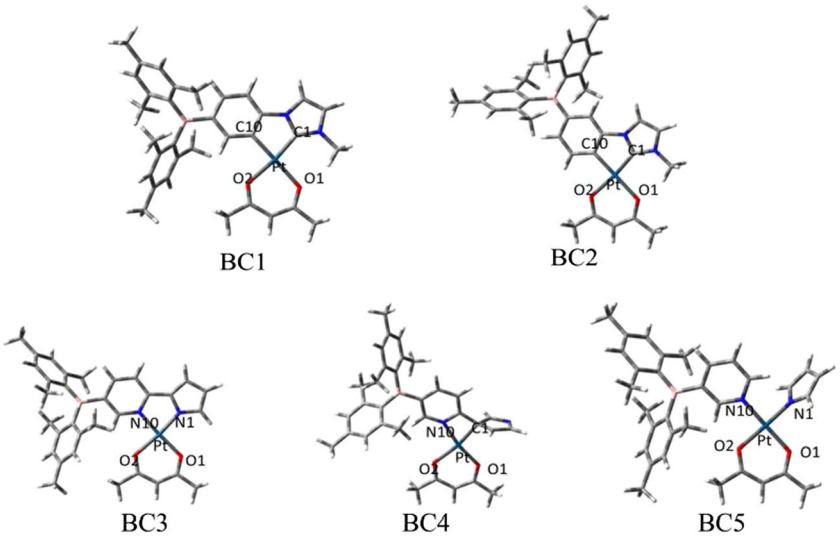

Fig. 1 Optimized ground state geometrical structures of studied complexes at the M06-2×/LANL2DZ level

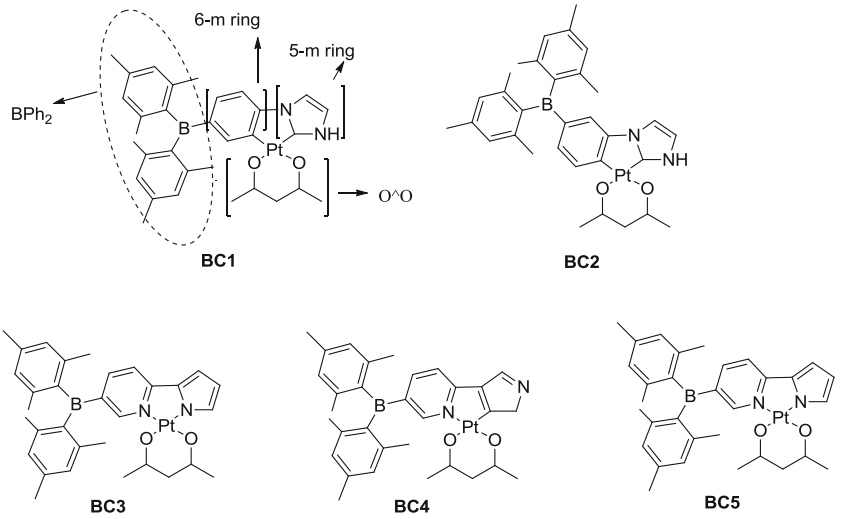

Fig. 2 Schematic structures of the investigated complexes

metal linearly as indicated from the calculated C10(C1)–Pt–O1(O2) angles around 175°. The optimized bond lengths and angles can be reproduced roughly by the crystal data but are slightly overestimated. In addition, it is worth noting that the Pt–C10 and Pt–N10 bond lengths are always longer than those of Pt–C1 and Pt–N1 except for BC4. It is well-known that the nature of the behavior of the metal-ligand toward an empty *d* orbital of the metal and a concurrent back-donation will from a filled d orbital to the π* antibonding orbital of the ligand. Because the pyrrole and imidazole groups have a stronger electron donation ability to the metal *d* orbital than benzene and pyridine groups, bonds are shorter and stronger. Generally, the calculated bond lengths are longer than the experimental data because the former are optimized in the gas phase and the latter are in a tight crystal lattice.

For the triplet excited state, T_1, the bond distances are shorter for Pt–C (N)10 and longer for Pt–C (N)1 bonds compared with those in the singlet state (S_0) as shown in Table 1. The change in these bonds indicates that, in the T_1 state, the interaction between the metal and the five-membered ring is strengthened, whereas the interaction between the metal and the boron ligand is weakened. According to the above analysis, we come to the conclusion that the structure of the ligand strongly affects the nature of the excited state.

Table 1 Selected optimized geometrical parameters of BC1–BC5 in the ground and lower lying triplet excited states at the M06-2×, respectively, together with the crystal data [4] of BC1 and BC2

		Bond length (Å)				Bond angle (deg)	
		Pt-C (1)	Pt-C (10)	Pt-O (1)	Pt-O (2)	C (1)-Pt-O (2)	C (10)-Pt-O (1)
BC1	S_0	1.94	1.97	2.18	2.11	172.0	178.7
	Exptl.	1.95	1.99	2.10	2.04	170.7	176.5
	T_1	1.94	1.97	2.18	2.11	172.8	177.8
BC2	S_0	1.94	1.97	2.18	2.12	173.2	179.5
	Exptl.	1.92	1.98	2.07	2.03	172.5	175.6
	T_1	1.94	1.92	2.17	2.12	173.6	179.4
		Pt-N (1)/C (7)	Pt-N (10)	Pt-O (1)	Pt-O (2)	N (1)/C (7)-Pt-O (2)	N (10)-Pt-O (1)
BC3	S_0	1.99	2.01	2.05	2.07	172.6	175.9
	T_1	2.00	2.01	2.05	2.04	172.5	175.9
BC4	S_0	1.99	2.02	2.03	2.12	168.1	167.9
	T_1	2.10	2.02	2.05	2.17	174.6	178.3
BC5	S_0	1.99	2.04	2.04	2.08	177.9	178.4
	T_1	2.04	2.02	2.06	2.02	176.9	179.8

Table 2 Calculated natural bond orbital (NBO) atomic charges q on the Pt (II) center in the S_0 and T_1 states

	$q(S_0)$	$q(T_1)$	$\Delta q(T_1\text{-}S_0)$
BC1	1.07	0.98	−0.09
BC2	1.07	1.12	−0.05
BC3	1.06	1.06	0
BC4	0.40	0.47	−0.07
BC5	0.81	0.80	0.01

The total natural bond orbital (NBO) charges on the Pt (II) center in the S_0 and T_1 states were calculated (Table 1). As shown in Table 2, the NBO charges on the Pt atom of 0.81e for BC5 are much less ionic than the formal Pt (II) ion and indicate considerable donation of electron density from the adjacent ligands to the Pt (II) *d* orbital. This also suggests that the pyrrole ligand is more efficient in transferring electrons from the *d* orbital of the Pt atom to the ligand on going from the singlet state to the triplet state than the imidazole ligand. This may lead to better charge transport ability than in the other four complexes.

Frontier molecular orbital properties

Because the observed differences in the optical and chemical properties of these complexes rely mainly on changes in the ground state electronic structure, we will discuss in detail the ground state electronic structure of these complexes with a special emphasis on the frontier molecular orbitals components, the HOMO and LUMO energy levels, and energy gaps. The frontier molecular orbital compositions and energy levels of BC1–BC5 are shown in Table S1–S5 and Fig. 3, respectively. Assignment of the type of each MO was made on the basis of its composition and by visual inspection of its three-dimensional representation.

As shown in Table S1–S5 and Fig. 3, the HOMO of BC1 is composed mainly of Pt *d* orbital (1.72 %), 6-membered ring (78.40 %), 5-membered ring (1.18 %) and the O^O segment (11.39 %). For BC2, the Pt *d* orbital (1.03 %), boron segment (25.09 %) and 6-membered ring (70.89 %) contribute to the composition. For BC3, the HOMO is composed mainly of boron segment (6.57 %), 6-membered ring (89.37 %) and 6-membered ring (3.75 %). For BC4, the *d* orbital (3.40 %) of Pt, the Boron segment (62.31 %), 6-membered ring (9.78 %), 6-membered ring (15.32 %) and O^O segment (9.20 %), respectively. Meanwhile the HOMO is composed mainly by Pt (4.21 %), and the 5-membered ring (83.72 %) in BC5. It is obvious in Fig. 3 that, in the HOMO, the Pt *d* orbitals are antibonding with the 6-membered rings and 5-membered rings for BC1–BC3. The O^O ligands do not play a significant role in the composition of HOMO for BC3 and BC5. But with respect to BC1, BC2 and BC4, the HOMO are essentially a π orbital on the O^O ligands. However, the HOMO is localized predominantly on the 6-membered rings except for BC4. It is notable that the contributions of 5-membered rings are changed in ascending order from BC1 to BC5. The compositions of the LUMO of BC1–BC5 are the π* orbital localized on the Boron segment and six-membered ring with more than

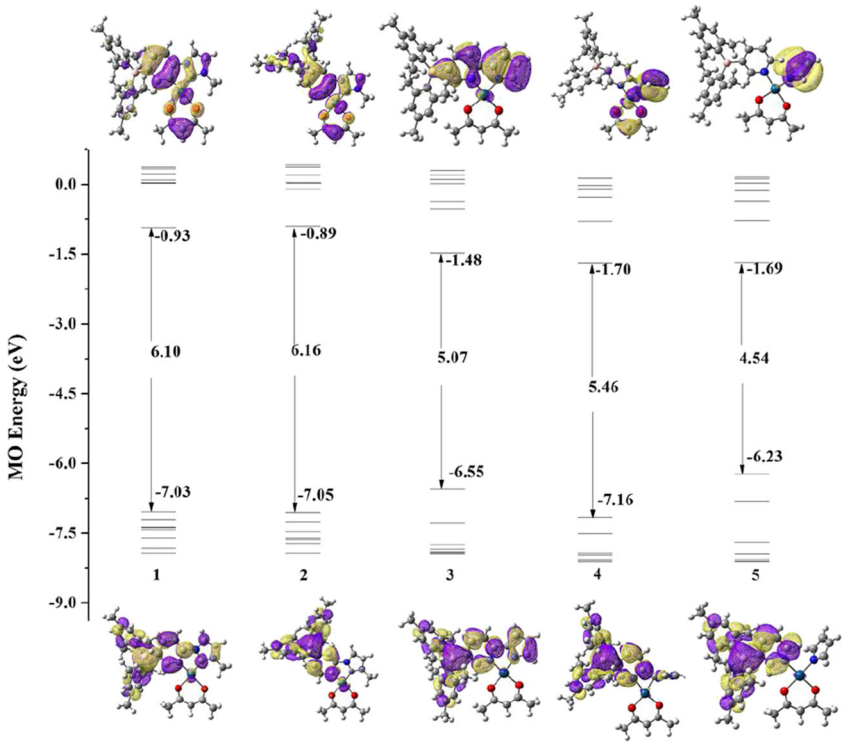

Fig. 3 Calculated energy-level diagram of the HOMOs and LUMOs for the studied complexes

Table 3 Absorptions of BC1–BC5 in dichloromethane (CH_2Cl_2) solution according to TDDFT (M06-2×) calculations. *H* HOMO, *L* LUMO

Complex	Transition	(CI coeff)	E (eV)/(nm)	Oscillator	Assign	Experimental (nm)
BC1	H→L	0.63194(67.90 %)	3.98/311	0.1490	MLCT/LLCT/ILCT	320
	H-2→L	0.62241(58.85 %)	4.20/295	0.1681	LLCT/ILCT	260
BC2	H→L	0.62161(66.53 %)	3.92/317	0.2719	MLCT/LLCT/ILCT	325
	H-2→L	0.60148(44.91 %)	4.09/303	0.1097	LLCT/ILCT	285
BC3	H→L	0.66354(86.72 %)	3.29/377	0.7892	MLCT/LLCT/ILCT	
	H-1→L+1	0.41910(30.05 %)	4.45/279	0.1349	LLCT/ILCT	
	H-1→L +2	0.38723(27.77 %)			LLCT/ILCT	
BC4	H→L	0.20480(28.19 %)	4.00/310	0.2084	MLCT/LLCT	
	H-1→L	0.14296(14.15 %)			MLCT/LLCT	
	H-3→L	0.58263(57.66 %)			MLCT/ILCT	
	H-4→H-1	0.35468(19.26 %)	4.68/265	0.1000	LLCT/ILCT	
	H-5→H-1	0.32781(17.80 %)			LLCT	
BC5	H-6→H-2	0.52615(50.09 %)	3.85/322	0.1432	LLCT	
	H-5→H-2	0.41620(39.62 %)			LLCT	
	H-4→H	0.25977(17.62 %)	4.52/274	0.1516	LLCT	
	H-5→H	0.44555(30.22 %)			LLCT	
	H-6→H	0.35647(24.17 %)			LLCT	

95 % composition, which show that the different ligands do not cause a significant change in LUMO distribution. However, the different ligands can tune the distribution of the HOMO orbital. This distribution will result in different electronic transition character upon excitation. The compositions of other lower occupied and higher virtual frontier MOs are similar to those of the HOMO and LUMO orbitals.

Moreover, the orbital energy levels of HOMO and LUMO are influenced by changing the ligands. As shown in Fig. 3, the HOMO level of BC3 and BC5 are more prominent than those of BC1, BC2 and BC4, and the order of stabilization of the HOMO energy levels is as follows: BC4(−7.16 eV)>BC2(−7.05 eV)> BC1(−7.03 eV)>BC3(−6.55 eV)>BC5(−6.23 eV), which means that pyrrole and pyridine ligands can raise the HOMO levels to benefit the hole-transporting ability in the resulting complexes relative to BC3 and BC5. This means that the pyrrole and pyridine ligands are good hole-transporting units. The LUMO energy levels of BC1 and BC2 are similar, which is consistent with the experimental observation that the photoluminescence spectra are similar. The LUMO energy levels of BC3(−1.48 eV), BC4(−1.70 eV) and BC5(−1.69 eV) are reduced compared to those of BC1(−0.93 eV) and BC2(−0.89 eV), which indicates that BC3, BC4 and BC5 have better electron injection ability than BC1 and BC2. The different hole-injection and electron-injection abilities will inevitably cause an influence on hole- and electron-injection balance and consequently affect device performance. We will discuss this aspect in detail in a later section. On the other hand, the HOMO–LUMO gaps of BC1(6.10 eV) and BC2(6.16 eV) are similar, while the HOMO–LUMO gaps of BC3(5.07 eV), BC4(5.46 eV) and BC5(4.54 eV) are significantly narrow. Therefore, this shows that different ligands can reduce the HOMO–LUMO gap and thus decrease the difficulty of electron transition from HOMO to LUMO or higher virtual MOs in the low-energy region. Likewise, this implies that the HOMO–LUMO transition may be the dominant configuration for the low-energy excitation of these complexes. As a result, investigation of the HOMO–LUMO gap will be helpful in understanding the variation trend of absorption and emission spectra.

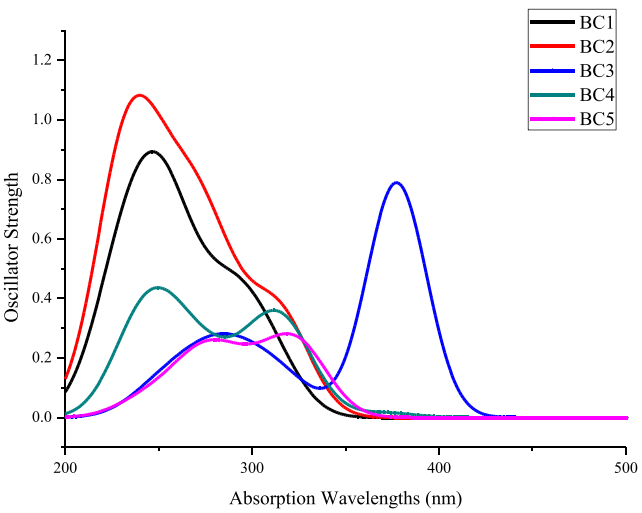

Fig. 4 Simulated absorption spectra of BC1, BC2, BC3, BC4 and BC5, respectively, in CH_2Cl_2 media

Absorption spectra

On the basis of the optimized ground-state geometry, the TDDFT/ M06-2×is method with PCM in CH_2Cl_2 media was used to calculate the absorption properties of the studied complexes. The calculated absorption spectra associated with their oscillator strengths, assignment, configurations, excitation energies, and excitations with maximum CI coefficients are listed in Table 3. For clarity, only the most leading excited states (with larger CI coefficients) are listed. The fitted absorption curve for BC1–BC5 as oscillator strength vs wavelength is depicted in Fig. 4.

As shown in Table 3 and Fig. 4, the lowest singlet absorptions of BC1–BC5 are calculated at 311, 317, 377, 310 and 322 nm, respectively. The lowest lying singlet to singlet absorption of BC3 and BC5 are markedly red-shifted compare to those of other complexes, which is consistent with the variation rules of the HOMO–LUMO energies gaps. This red shift of the longer wavelength band is attributed to the intense participation of the pyrrole and pyridine ligands. BC4 also has the pyrrole and pyridine ligands, however, the N atom of pyrrole does not coordinate directly with the Pt atom, which would weaken the interaction between the metal and its ligands. According to Tables S1–S2 and Figs. S1–S2 in the supporting information, we can draw the conclusion that the transition at 311 nm for BC1 and the transition at 317 nm for BC2 can be described as [d (Pt)+π (6-m ring)+π (5-m ring)+π (O^O)]→[π*(6-m ring)+π*(5-m ring)+π*(Bph_2)] transition with MLCT/LLCT/ILCT character, while the transition at 295 and 303 nm can be described as [π (Bph_2)]→[π*(6-m ring)+π*(Bph_2)] transition with LLCT/ILCT character for BC1 and BC2, respectively. Thus, the similar absorption spectra depend on the similar transition characters as shown in Fig. 4. For BC3 (referring to Table S3 and Fig. S3), the lowest lying transition at 377 nm is attributed to [d (Pt)+π (6-m ring)+π (5-m ring)]→[π*(6-m ring)+π*(5-m ring)+π*(Bph_2)] transition with the character of MLCT/LLCT/ILCT, while the transition at 279 nm is attributed to [π (5-m ring)+π (O^O)]→[π*(6-m ring)+π*(O^O)] transition with the character of LLCT/ILCT. For BC4 (referring to Table S4 and Fig. S4), the lowest lying transition at 310 nm is attributed to [d (Pt)+π (5-m ring)+π (O^O)]→[π*(6-m ring)+π*(Bph_2)], [d (Pt)+π (5-m ring)+π (O^O)]→[π*(6-m ring)+π*(Bph_2)] and [d (Pt)+π (5-m ring)+π (Bph_2)]→[π*(6-m ring)+π*(Bph_2)] transition with the character of MLCT/LLCT, MLCT/LLCT and MLCT/ILCT, respectively. But the transition at 265 nm is attributed to [π (5-m ring)+π (Bph_2)]→[π*(5-m ring)+π*(O^O)] and [π (Bph_2)]→[π*(5-m ring)+π*(O^O)] transition with the character of LLCT/ILCT and LLCT, respectively. It is attributed to [π (Bph_2)]→[π*(O^O)] transition with the single character of LLCT at 322 nm, while it is attributed to [π (Bph_2)]→[π*(5-m ring)] transition with the single character of LLCT at 274 nm for BC5 (according to Table S5 and Fig. S5). The experimentally observed strongest absorptions localized at higher energy regions are 320, 260 nm (BC1) and 325, 285 nm (BC2) in CH_2Cl_2, respectively. The calculated outcomes are good agreement with the experimental values.

The calculated results agree with the experimental observations that the MLCT component exists in the lower energy region. This is due to the presence of heavy metal effects involved in these complexes, which can produce lower energy absorptions. Though the absorption of MLCT is weak, the participation of metals in these complexes probably makes the transition occur and therefore enhances the luminescence quantum yields. Moreover, different ancillary ligands can cause different excitation energy and transition character. Therefore, modification of the ligand structure can tune the photo physics and luminescent characteristics.

Ionization potentials and electron affinities

In order to understand the charge injection and transporting properties of luminescent materials, we calculated ionization potentials (IP), electron affinities (EA), reorganization energy (λ), hole extraction potential (HEP) and electron extraction potential (EEP) for the studied complexes (shown in Table 4). The IP and EA are used to evaluate the energy barrier for the injection of holes and electrons, respectively [33]. IP and EA are either vertical excitations (v; at the geometry of the neutral molecule) or adiabatic excitations (a; optimized structure for both the neutral and charged molecules). HEP is the energy difference between M (neutral molecule) and M^+ (cationic), using M^+ geometry. EEP is the energy difference between M and M^- (anionic), using M^- geometry. Generally speaking, the lower the IP of the emitter, the easier injection of holes from the hole-transporting layer (HTL) to the emitter is. The higher the EA of the emitter, the easier injection of electrons from the electron-transporting layer (ETL) is. Materials with low IP

Table 4 Ionization potential (IP), electronic affinity (EA), hole extraction potential (HEP) and reorganization energies (EEP) for each molecule (in eV) calculated using the M06-2× method

	IP (*v*)	IP (*a*)	HEP	EA (*v*)	EA (*a*)	EEP	λ_{hole}	$\lambda_{electron}$	△λ
BC1	7.44	7.23	7.00	0.63	0.76	0.87	7.21	1.00	6.21
BC2	7.45	7.21	6.97	0.61	0.74	0.86	7.21	1.00	6.22
BC3	7.06	6.87	6.68	1.18	1.30	1.41	6.87	1.53	5.34
BC4	7.74	6.65	6.00	1.37	1.53	1.68	7.09	1.84	5.25
BC5	6.91	6.47	6.11	1.41	1.56	1.69	6.55	1.85	4.70

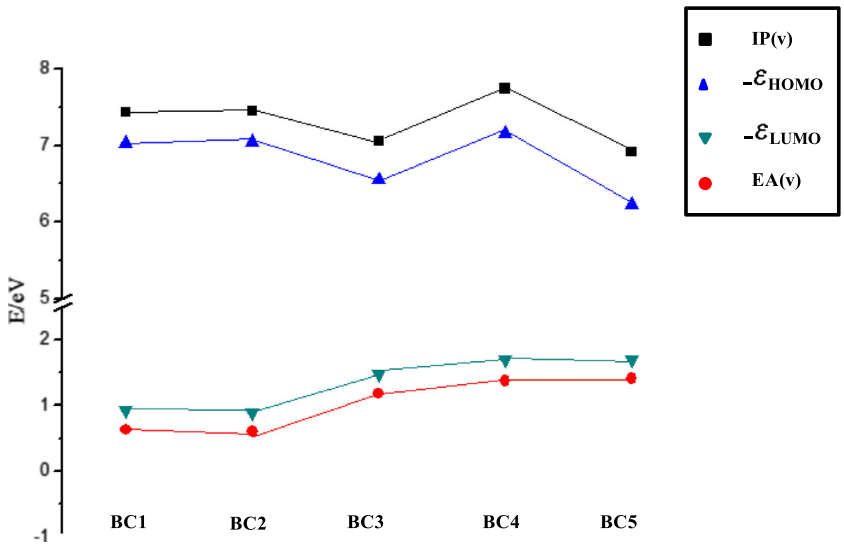

Fig. 5 Calculated negative values of HOMO and LUMO energy levels, ionization potentials (IP; v), and electronic affinities (EA; v) of the complexes

and high EA can decrease the turn-on voltage and improve the performance of devices.

The calculated EA (*v*), EA (*a*), and EEP increase from BC1 to BC5 (shown in Table 4), in accordance with the order of the absolute values of HOMO energies (shown in Fig. 3). The highest EA (1.56 eV) is found for BC5, suggesting that complex BC5 is the easiest for electron injection, while BC1 is observed to be the most difficult for electron injection. The calculated IP (*v*), and IP (*a*) decrease from BC1 to BC5. The IP values of BC1 and BC2 are similar so that the hole injection ability of these two geometric isomers are about the same. Changing the structure from BC3 to BC5 significantly lowers the IP (*v*) and IP (*a*), and enhances the device's efficiency. It is noteworthy that complex BC5 has the most favorable IP and EA values compared with other complexes, which will not only enhance the hole-transporting ability but also enhance the electron-transporting ability. Thus, the molecule we designed can deliver the most balanced charge transport and enhance nonradiative recombination because of interactions of excitons with the charge carriers.

According to the Maecus/Hush model [34–36], the charge (hole or electron) transfer rate, *k*, can be expressed by the following formula:

$$k = \left(\frac{\pi}{\lambda k_b T}\right)^{1/2} \frac{V^2}{\hbar} exp\left(-\frac{\lambda}{4k_b T}\right) = Aexp\left(-\frac{\lambda}{4k_b T}\right) \quad (1)$$

Where T is the temperature, k_b is the Boltzmannn constant, λ is the reorganization energy, and V is the coupling matrix element between the cation and molecules, which is dictated by the overlap of orbitals. Obviously, the reorganization energy in the charge transfer process is very important. As shown in Table 4, the $\lambda_{electron}$ values are all smaller than the λ_{hole} values, which suggests that the electron transfer rate is better than the hole transfer rate. The difference between $\lambda_{electron}$ and λ_{hole} decreases from BC1 to BC5 ($\triangle\lambda$: 6.21≈6.22<5.34<5.25<4.70), which indicates that introduction of pyrrole onto the metal Pt atom can greatly improve the charge transfer balance, thus further enhancing the device performance of OLEDs.

The variations in negative values of HOMO and LUMO energy levels, IP (v), and EA (v) of the complexes are shown in Fig. 5. The negative value of the HOMO energy level is lower than IP, but the negative value of the LUMO energy level is higher than EA. Therefore, the HOMO energy level underestimates the ability to lose an electron, whereas the LUMO overestimates the ability of electron capture. Nevertheless, the order of the abilities to lose or capture an electron predicted by the HOMO and LUMO energy levels is correct for a series of studied complexes. The above analysis of the variation trend of the HOMO and LUMO, and the charge transfer rate of holes and electrons, suggests that the performance of OLED can be influenced greatly by the ancillary ligands. The calculated results confirm earlier information that the device performance can be changed easily by modifying or tuning the substituents. This a key point toward the development of novel transition metal-containing materials for OLEDs.

Table 5 Calculated emission energies of T_1 and their transition nature for complexes BC1–BC5

	λ (nm)/ E (eV)	Configuration	Assign	Experimental (nm)
BC1	452/2.52	L→H (0.41)	MLCT/LLCT/ILCT	478
BC2	420/2.87	L→H (0.67)	MLCT/LLCT/ILCT	462
BC3	507/2.05	L→H (0.91)	MLCT/LLCT/ILCT	
BC4	600/2.77	L→H (0.64)	MLCT/LLCT	
BC5	539/1.82	L→H (0.70)	MLCT/LLCT	

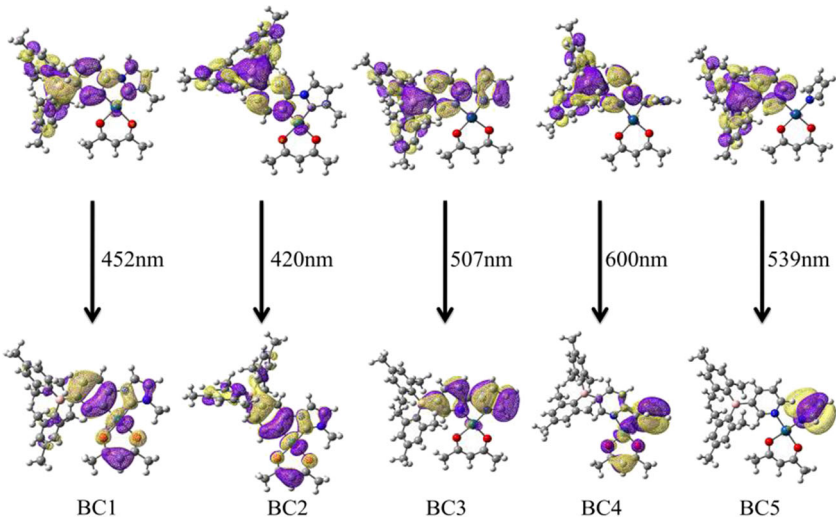

Fig. 6 Transitions responsible for the emissions at 420, 452, 507, 600 and 539 nm for complexes BC1–BC5, respectively, simulated in CH_2Cl_2 media

Phosphorescence in CH_2Cl_2 media and the PL quantum efficiency

The phosphorescent spectra in CH_2Cl_2 media were calculated by TD-DFT on the basis of the lowest triplet state (T_1) geometries. The calculated emission energies, dominant configurations (with larger CI coefficients), transition nature, and the available experimental values are listed in Table 5. For clarity, the plots of the molecular orbitals related to emissions of BC1–BC5 are presented in Fig. 6.

The calculated phosphorescence at 452 and 420 nm of BC1 and BC2 agree with the corresponding experimental values 478 and 462 nm, respectively. For BC3–BC5, the calculated emissions are at 507, 600 and 539 nm, respectively. Table 5 and Fig. 6 show that the emissions of the complexes BC1 to BC5 are contributed mainly by LUMO→HOMO transition.s The emission for the complexes are BC4(600 nm)> BC5(539 nm)>BC3(507 nm)>BC1(452 nm)> BC2(420 nm), indicating that the emission properties are very sensitive to the selected ancillary N-heterocyclic carbine (NHC) in these five complexes. And, more remarkably, the NHC-chelate Pt (II) complexes BC1, BC2, BC3 and BC5 display highly efficient blue and blue-green phosphorescence in CH_2Cl_2 solution.

In principle, the phosphorescence quantum yield Φ_p from an emissive excited state to the ground state is related directly to the radiative (k_r) and nonradiative (k_{nr}) rate constants by Eq. (2).

$$\Phi_p = \frac{k_r}{k_r + k_{nr}} \tag{2}$$

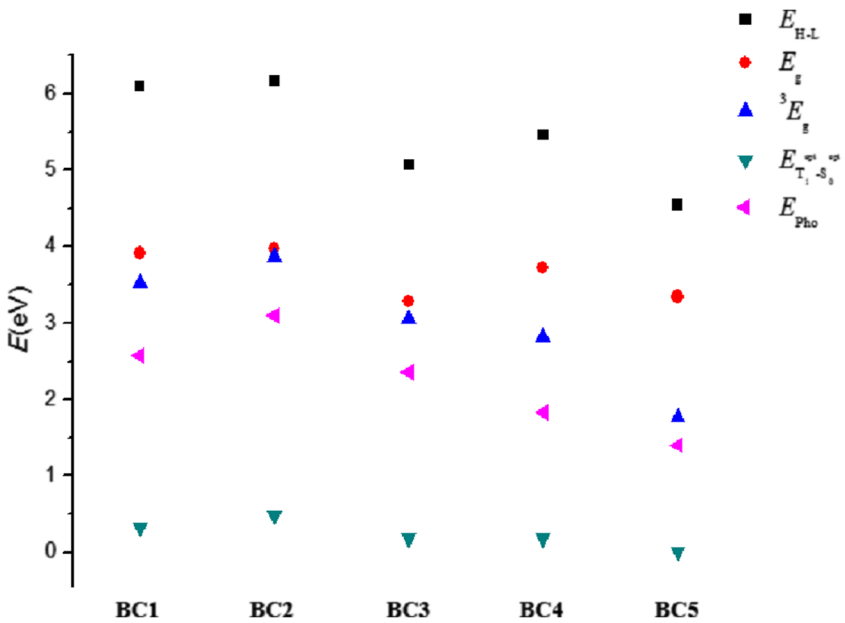

Fig. 7 Variation of the HOMO–LUMO gaps $E_{H\text{-}L}$, the minimum emission energy of phosphorescence E_{Pho}, the energy difference between the relaxed S_0 and T_1 geometries, $E_{T_1^{opt}} - E_{S_0^{opt}}$ and lowest singlet-singlet (E_g) and singlet-triplet (^3E_g) vertical transition energies on the basis of the S_0 states of the complexes

Therefore, the quantum yield Φ_p can be improved by increasing k_r and/or decreasing k_{nr}. The nonradiative rate constant k_{nr} from the T_m state to the S_0 state can be expressed as Eq. (3) [37, 38, 39].

$$k_{nr}(T_m \rightarrow S_0) \propto \exp\left\{-\beta\left[E\left(T_m - E(S_0)\right]\right\}\right. \quad (3)$$

This increases with increasing structural distortion (β parameter) and decreasing energy difference between the T_m and S_0 states. Small k_{nr} values are conducive to developing effective phosphorescent materials.

As shown in Fig. 7, the energies of phosphorescence E_{Pho}, the energy difference between the relaxed S_0 and T_1 geometries $\left(E_{T_1^{opt}} - E_{S_0^{opt}}\right)$, and the singlet-triplet vertical transition energies ${}^3E_g$ on the basis of the S_0 geometry follow the same trend. Figure 7 also shows that the Stokes shifts between ${}^3E_g$ and E_{Pho} for BC5 is smallest in these complexes. A small Stokes shift may be favorable to strong phosphorescence [40, 41]. According to the data in Fig. 7, the following can be inferred from Eq. (3): the $T_1^{opt} - S_0^{opt}$ energy gap of BC5 is slightly smaller than other complexes. Hence, we can forecast that BC5 may have highest phosphorescence quantum yield in these five complexes. This is consistent with the above analysis. All in all, pyrrole-functionalized Pt complex shows higher phosphorescence quantum yield than other complexes.

Conclusions

We investigated the structures, absorptions, transporting abilities, and phosphorescent properties of five Pt (II) complexes using DFT. The calculated results reveal that, for these five NHC-chelate Pt (II) compounds, the electron-transporting performance is better than the hole-transporting performance. Notably, the pyrrole ligand on the metal center in BC5 has a significant influence on the charge transport ability, and has the best balanced charge transport ability among the studied complexes. Moreover, we can forecast that BC5 may have highest phosphorescence quantum yield of these five complexes. We hope that our study will aid better understanding of the structure–property relationship of phosphorescent Pt (II) complexes and provide constructive information for designing novel and highly efficient OLED materials in the future.

Acknowledgments The authors are grateful for financial aid from the National Natural Science Foundation of China (Grant Nos. 21371165, 51372242, 91122030 and 21210001), National Natural Science Foundation for Creative Research Group (Grant No. 21221061), Jilin Province Youth Foundation (201201008), and Computing Center of Jilin Province.

References

1. Lin JJ, Liao WS, Huang HJ, Wu F, Cheng CH (2008) Adv Funct Mater 18:485–491
2. Chen K, Yang CH, Chi Y, Liu CS, Chang CH, Chang CC, Wu CC, Chung MW, Cheng YM, Lee GH, Chou PT (2010) Chem Eur J 16: 4315–4327
3. Wang L, Wu Y, Shan GG, Geng Y, Zhang JZ, Wang DM, Yang GC, Su ZM (2014) J Mater Chem C 2:2859–2868
4. Wong WY, Ho CL (2009) J Mater Chem 19:4457–4482
5. Wang J, Bai FQ, Xia BH, Zhang HX, Tian C (2014) J Mol Model 20: 2018–2027
6. Arduengo AJ III, Harlow RL, Kline M (1991) J Am Chem Soc 113: 361–363
7. Sajoto T, Djurovich PI, Tamayo A, Yousufuddin M, Bau R, Thompson ME, Holmes RJ, Forrest SR (2005) Inorg Chem 44: 7992–8003
8. Holmes RJ, Forrest SR, Sajoto T, Tamayo A, Djurovich PI, Thompson ME, Brooks J, Tung YJ, D'Andrade BW, Weaver MS, Kwong RC, Brown J (2005) Appl Phys Lett 87:243507–243510
9. Chang CF, Cheng YM, Chi Y, Lin CC, Lee GH, Chou PT, Chen CC, Chang CH, Chen CC, Wu CC (2008) Angew Chem Int Ed 47:4542–4545
10. Haneder S, Da Como E, Feldmann J, Lupton JM, Lennartz C, Erk P, Fuchs E, Molt O, Munster I, Schildknecht C, Wagenblast G (2008) Adv Mater 20:3325–3330
11. Hsieh CH, Wu FI, Fan CH, Huang MJ, Lu KY, Chou PY, Ou Yang YH, Wu SH, Chen IC, Chou SH, Wong KT, Cheng CH (2011) Chem Eur J 17:9180–9187
12. Sasabe H, Takamatsu J, Motoyama T, Watanabe S, Wagenblast G, Langer N, Molt O, Fuchs E, Lennartz C, Kido J (2010) Adv Mater 22:5003–5007
13. Unger Y, Meyer D, Molt O, Schildknecht C, Münster I, Wagenblast G, Strassner T (2010) Angew Chem Int Ed 49: 10214–10216
14. Lu KY, Chou HH, Hsieh CH, Ou Yang YH, Tsai HR, Hsu LC, Chen CY, Chen IC, Cheng CH (2011) Adv Mater 23:4933–4937
15. Unger Y, Meyer D, Strassner T (2010) Dalton Trans 39:4295–4301
16. Zhang X, Wright AM, DeYonker NJ, Hollis TK, Hanmmer NI, Webster CE, Valente EJ (2012) J Organometallics 31: 1664–1672
17. Fukagawa H, Shimizu T, Hanashima H, Osasa Y, Suzuki M, Fujikake H (2012) Adv Mater 24:5099–5103
18. Rausch AF, Thompson ME, Yersin H (2009) Chem Phys Lett 468: 46–51
19. Rausch AF, Yersin H (2010) Chem Phys Lett 484:261–265
20. Fleetham T, Wang ZX, Li J (2012) Org Electron 13:1430–1435
21. Hudson ZM, Sun C, Helander MG, Chang YL, Lu ZH, Wang S (2012) J Am Chem Soc 134:13930–13933
22. Zhao Y, Truhlar DG (2008) Theor Chem Accounts 120:215–241
23. Autschbach J, Ziegler T, Gisbergen SJA, Baerends EJ (2002) J Chem Phys 116:6930–6940
24. Helgaker T, Jørgemsen P (1991) J Chem Phys 95:2595–2601
25. Bak K, Jørgemsen LP, Round TK, Jensen HJA (1993) J Chem Phys 98:8873–8887
26. Canc'es E, Mennucci B, Tomasi J (1997) J Chem Phys 107:3032–3041
27. Cossi M, Barone V, Mennucci B, Tomasi J (1998) Chem Phys Lett 286:253–260
28. Mennucci B, Tomasi J (1997) J Chem Phys 106:5151
29. Hay PJ, Wadt WR (1985) J Chem Phys 82:270–283
30. Wadt WR, Hay PJ (1985) J Chem Phys 82:284–298

31. Hariharan PC, Pople JA (1974) Mol Phys 27:209–214
32. Frisch MJ, Trucks GW, Schlegel HB, Scuseria GE, Robb MA, Cheeseman JR, Scalmani G, Barone V, Mennucci B, Petersson GA et al (2010) Gaussian 09, Revision B. 01. Gaussian, Inc., Wallingford, CT
33. Li XN, Wu ZJ, Si ZJ, Zhang HJ, Zhou L, Liu XJ (2009) Inorg Chem 48:7740–7749
34. Hush RA (1958) J Chem Phys 28:962–972
35. Marcus RA (1956) J Chem Phys 24:966
36. Marcus RA (1993) Rev Mod Phys 65:599–610
37. Tong GS, Che CM (2009) Chem Eur J 15:7225–7237
38. Wilson JS, Chawdhury N, Al-Mandhary MRA, Younus M, Khan MS, Raithby PR, Köhler A, Friend RH (2001) J Am Chem Soc 1239412. b) H. Yersin, W. J. Finkenzeller, in Highly Efficient OLEDs with Phosphorescent Materials (Ed.: H. Yersin), Wiley-VCH, Weinheim, 2008, pp. 163.
39. Yersin H, Finkenzeller WJ (2008) Triplet emitters for OLEDs—basic properties. In: Yersin H (ed) Highly efficient OLEDs with phosphorescent materials. Wiley-VCH, Weinheim, pp 163
40. Dedeian K, Shi J, Shepherd N, Forsythe E, Morton DC (2005) Inorg Chem 44:4445–4447
41. Otterstedt JEA (1973) J Chem Phys 58:5716